Progress In Electromagnetics Research, Vol. 111, 291–309, 2011

EXPERIMENTAL DYNAMICAL EVOLUTION OF THE BRILLOUIN PRECURSOR FOR BROADBAND WIRELESS COMMUNICATION THROUGH VEGETATION

A. V. Alejos, M. Dawood, and L. Medina †

Klipsch School of Electrical and Computer Engineering
New Mexico State University
Las Cruces, NM 88003, USA

Abstract—In this paper, we report experimental results on detecting and analyzing the Brillouin precursor through vegetation at frequencies from 500 MHz to 3 GHz. An experimental method to collect data is reported. The outcomes in terms of energy and time-spreading are presented using modulated rectangular and Gaussian pulses, as well as a sequence of rectangular pulses. Using field-collected data, this study shows the estimated dynamical evolution of the Brillouin precursor fields for wideband wireless systems, such as those represented by IEEE 802.16. The advantages of Brillouin precursors in terms of power spectrum density and bit energy are discussed. Complex relative permittivity is extracted from the experimental data and is used in theoretical formulation to analyze dispersive propagation for any kind of input waveform. Finally, a near-optimal pulse is proposed to achieve maximum propagation distance and/or signal-to-noise ratio for the transmission of bit stream sequences through vegetation.

1. INTRODUCTION

The electromagnetic (EM) waves propagating through natural dispersive media, such as soil, foliage, water, etc., experience frequency-dependent attenuation and phase distortion. These effects alter the structure of the EM propagating fields through such media. This alteration is more pronounced for ultrawideband (UWB) and/or ultrashort pulses, resulting in the formation of fields called Somerfeld and Brillouin precursors [1–4]. In general, EM signals

Received 7 October 2010, Accepted 22 November 2010, Scheduled 9 December 2010
Corresponding author: Ana Vazquez Alejos (analejos@uvigo.es).
† A. V. Alejos is also with Signal Theory and Communications Department, University of Vigo, Vigo 36310, Spain.

with superimposed Brillouin precursor field undergo algebraic peak amplitude decay instead of the exponential decay. Therefore, a propagating EM wave having a Brillouin precursor component can achieve larger penetration depths into a dispersive medium, compared to that of the conventional single frequency or narrow-band signals, thereby offering better signal-to-noise ratio (SNR) and/or enhanced propagation distances.

The formation of the Brillouin precursor and its resulting lower attenuation through dispersive media are particularly useful in underground, undersea/ice communications, for both military and civil applications. For instance, it can benefit the underground sensor networks for monitoring soil parameters such as humidity and salinity in agriculture. Another example could be the sensor networks deployed within forests and dense foliage.

The new and emerging radio communication systems use even larger bandwidths to achieve higher data rates for various applications. Thus, the propagation medium that is normally considered non-dispersive may necessarily be considered as dispersive. The use of precursors could be advantageous in terms of either same range and less power consumption or longer range for the same power. Therefore it would impact positively radio budget links, transmission data rate, number of users, etc.. For example, the use of Brillouin precursors could improve the radio link range in forests. It could contribute to "green technologies" providing the same range and data transmission capacities with reduced transmitted power. It also seems appropriate to use precursors in radio-link budget analysis, and in designing appropriate transmitters and receiver structures [5].

To date, there are only a few experimental studies regarding the use of precursors at microwave frequencies [6]. None of these are related to the radio channel consisting of vegetation or foliage [6, 7]. The experimental verification of the existence of the Brillouin precursors through such channels at microwave frequencies is therefore of vital importance for applications in wideband wireless communications, such as those represented by the standard IEEE 802.16.

In our previous studies [7], we used a frequency-domain experimental method to obtain the material response to an incoming EM signal. These data were also used to calculate the complex relative dielectric permittivity $\varepsilon_r(\omega)$ of the underlying dispersive material [8, 9]. The estimated permittivity $\hat{\varepsilon}_r(\omega)$ together with the theoretical formulation in [10] was used to predict the dynamical evolution of any kind of input pulse traveling through the material. Both theoretical and experimental methods have been used to detect and analyze the Brillouin precursor corresponding to sine-modulated

rectangular and Gaussian pulses, as well as for a modulated sequence of rectangular pulses.

The experimental results in this paper discuss the advantages of the Brillouin precursor for various waveforms in terms of peak amplitude, power spectrum density (PSD), and bit energy (E_b), thereby providing an indication in terms of bit error rate (BER) improvement. These results are important because we used actual vegetation, a nonhomogeneous medium, in contrast with the simulation studies using theoretical and/or empirical models representing homogeneous media with spatial continuity. Moreover, the results in this paper are slightly polarizationdependent due to the non-isotropic nature of the vegetation used in this study.

We further show the effect of dispersion in terms of pulse broadening for a sequence of rectangular pulses representing an information-bearing stream. Due to the polidispersive nature of the actual vegetation, it is shown that the spreading effect is less critical than the one predicted by theoretical dielectric models [2, 11].

Section 2 briefly describes the experimental method used in this study. The experimental results to detect the precursor formation for rectangular and Gaussian transmit pulses through vegetation are presented and discussed in Section 3. Section 4 briefly addresses the extraction of the complex dielectric relative permittivity $\hat{\varepsilon}_r(\omega)$ of the vegetation media under study. The estimated relative dielectric permittivity is then used in theoretical formulation to analyze the dynamical evolution of a sequence of rectangular pulses in terms of peak amplitude decay and pulse broadening. Section 5 illustrates the evolution of the power spectrum density and the bit energy vs. propagation distance. In Section 6, we propose an alternate pulse for near-optimal propagation through vegetation. Finally, conclusions are offered in Section 7.

2. EXPERIMENTAL DATA COLLECTION METHOD

The experimental method described herein is composed of a system set-up, a measurement procedure, and a data processing technique, analogous to a free-space dielectric properties measurement system [7–9]. Fig. 1 shows the geometry of the experimental setup. The propagation channel is a *False Cypress* (Kochia Scoparia) tree depicted in Fig. 2. Measurements were conducted in an outdoor environment with absorbing material placed on the ground between the tree and each antenna to mitigate the ground reflections. The tree is located in the northern part of the New Mexico State University campus, Las Cruces, USA.

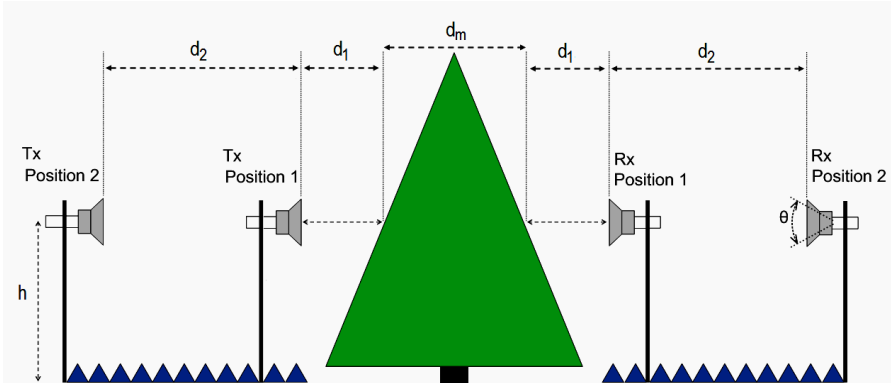

Figure 1. Geometry of experimental set-up.

Figure 2. Picture of the actual *Kochia Scoparia* tree utilized in the experiment.

The Agilent Technologies E8362B PNA was used to collect the $s_{21}(f)$ parameters through free-space and through the tree. A low noise amplifier (LNA) having a power gain of 25 dB over 10 MHz to 6 GHz with a flatness level of ± 1.5 dB was used in the transmitter chain. Another similar LNA with 15 dB power gain was used in the receiver chain. A set of two quad rigid horn antennas with a 60° 3-dB beamwidth, identical gains and radiation patterns were used to cover the frequency band from 500 MHz to 3 GHz. The experimental data were collected using +10 dBm transmitted power, with 4600 points,

140 ms sweep time, and an averaging factor of 50.

The selected separation distance $d_1 + d_2$ was 4.78 m, enough to guarantee far field (FF) conditions at the specified frequencies. For near field (NF) measurements, d_1 was 0.78 m. Both transmit and receive antenna heights were $h = 1.5$ m. The tree depth d_m was 7.62 m, measured at the height h above the ground.

The frequency response $s_{21\_air}(f)$, and $s_{21\_veg}(f)$ are collected, respectively, for the air (free space) propagation conditions, and with the tree placed between the antennas. The $s_{21}(f)$ raw data were collected at normal incidence using both horizontal-horizontal (HH) and vertical-vertical (VV) co-polarizations, for three transmitter (tx) and receiver (rx) antenna configurations, namely: tx and rx in NF (NF-NF), tx in FF and rx in NF (FF-NF), both tx and rx in FF (FF-FF).

The parameter s_{21} measures the ratio of the received electric field $E_2 = E_0 \cdot e^{-\gamma \cdot d}$ (at port 2) to the transmitted electric field $E_1 = E_0$ (at port 1) such that $s_{21} = E_2/E_1 = (E_0 \cdot e^{-\gamma \cdot d})/E_0$. The γ and d are, respectively, the propagation constant and the distance through the dispersive media. The traveled distance d varies according the media thickness placed between the transmitter and the receiver, and also for near field or far field conditions. The same applies to the propagation constant γ, which also depends on the EM wave polarization. The result is a set of s_{21} responses for each combination of distance and polarization.

A Power-Delay-Profile (PDP) is obtained by applying an Inverse Fast Fourier Transform (IFFT) to the s_{21} raw data. The PDP would ideally show just one peak corresponding to the direct component of the normal transmission. However, spurious components, such as multipaths, will result in additional minor peaks in the PDP [8, 12, 13], thereby contaminating the propagated waveform. In order to remove the undesired components, a time-gating filter is applied to the experimental PDP [8, 12]. We used a Gaussian time-gating filter, $g(t) = \exp\{-[(t-a)/b]^2\}$, with a shape close to the ideal PDP. The parameter a can be adjusted to correspond to the direct received component. Parameter b is chosen to ensure that most of the energy in the main peak of the PDP is retained after filtering.

The next step is to obtain the ratio between the time-gated responses $s_{21\_veg}(f)$ and $s_{21\_air}(f)$, providing a general propagation factor $T_{s21}(f)$ that incorporates the frequency-dependent response in terms of amplitude and phase effects on the signal propagated through

the dispersive medium. It can be shown that:

$$s_{21\_veg} = \frac{E_0 \cdot e^{-\gamma_0 \cdot d_i} \cdot \tau_{av} \cdot e^{-\gamma_m \cdot d_m} \cdot \tau_{va} \cdot e^{-\gamma_0 \cdot d_j}}{E_0} \tag{1}$$

$$s_{21\_air} = \frac{E_0 \cdot e^{-\gamma_0 \cdot d_i} \cdot e^{-\gamma_0 \cdot d_m} \cdot e^{-\gamma_0 \cdot d_j}}{E_0} \tag{2}$$

$$T_{s21} = \frac{E^r_{veg}/E_0}{E^r_{air}/E_0} = \frac{s_{21\_veg}}{s_{21\_air}} = \tau^2_{av} \cdot e^{-d_m \cdot (\gamma_m - \gamma_0)} \tag{3}$$

where γ_0 and γ_m are the propagation constants through air, and the dispersive dielectric material, respectively; τ_{av} and τ_{va} are the transmission coefficients for the air-vegetation and vegetation-air interfaces, respectively; d_i, d_j are the separation distances for the transmitter and receiver antennas, with $i, j = 1, 2$, as depicted in Fig. 1; and d_m is the tree depth, 7.62 m. Assuming reciprocity, $\tau_{av} = \tau_{va}$. It may be noted that $T_{s21}(f)$ does not represent a transmission coefficient due to be referred to the same point, the receiver. This was the reason to name it as propagation factor.

The transmission coefficient τ_{av} is obtained experimentally using the reflection parameter s_{11_veg}, leading to the expression $\tau_{av} = 1 + \rho_{av}$, with ρ_{av} being the reflection coefficient of the air-vegetation interface. For our case, a two port network, transmitter as input and receiver as output, ρ_{av} is given by the parameter s_{11_veg}. This leads to $\tau_{av} = 1 + s_{11\_veg}$. The measured s_{11_veg} was also time gated to ensure that only the desired direct signal component is present.

The expression $T_{s21}(f)$ in (3) can be considered a filter response function in frequency domain, provided identical plane references for all the considered distance and polarization configurations are maintained. That expression eliminates most of the involved $e^{-\gamma \cdot d}$ terms and this further simplifies the method to obtain the dispersive material propagation constant γ_m. The final general propagation factors $T_{s21}(f)$ corresponding to both polarizations and all distance conditions are shown in Fig. 3. It may be observed that the results confirm an almost identical trend for all configurations.

The time-gating process applied to various collected $s_{21}(f)$ frequency responses guarantees that only the direct component is present in the power-delay-profile (PDP). Under these conditions, the Fresnel model [12] can be assumed to explain the propagation inside the material as $e^{-\gamma_m \cdot d_m}$. The Fresnel transmission model is valid for the case containing a predominant direct component, or for a largely lossy material which also ensures minimal multipath. Other propagation models given by the internal multireflection model (IMR) [12, 13] can also be assumed. In this case, the time-gating may not be needed, and both multipath and direct components must be considered.

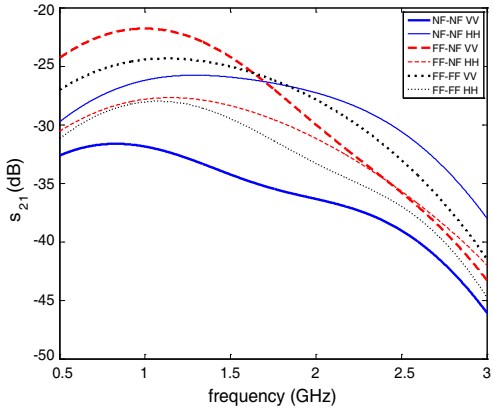

Figure 3. Time gated s_{21_veg} data for all configurations.

3. EXPERIMENTAL RESULTS

The general propagation factor $T_{s21}(f)$ can be interpreted as a filter that models the behavior of the different spectral components of an EM signal traveling through it. Assuming an input pulse $p(t)$ with its frequency response $P(f)$, modulated at some carrier frequency f_0, the output signal in the frequency and time-domain, respectively, would be $Y(f) = P(f) \cdot T_{s21}(f)$ and $y(t) = p(t) \otimes \text{IFFT}\{T_{s21}(f)\}$, with IFFT$\{\cdot\}$ and $\otimes$ denoting the inverse Fourier transform and the convolution operations, respectively. The output signal, $y(t)$, offers the dynamical evolution of the pulse $p(t)$ after traveling through the foliage. It may also be noted that this process can be used for any type of waveforms, including pulses or sequence of pulses, coded and/or non-coded. In addition, parameters controlling the pulse shape and the carrier frequency can be changed, within the constraints given by the bandwidth considered during the measurement process.

Shown in Figs. 4–6 are the results corresponding to all polarization and distance conditions for one sine-modulated rectangular pulse and one Gaussian pulse of duration $T_b = 10/f_0$ at carrier $f_0 = 2.5\,\text{GHz}$. One may observe the appearance of the Brillouin precursor in the leading and trailing edges of the rectangular pulse, as well as in the leading edge of the Gaussian pulse. It may further be noticed that the rectangular pulse offers a better choice for the formation of the Brillouin precursor at both its leading and trailing edges due to the larger number of spectral components present therein. On the other hand, the Gaussian pulse shows an infinitely long smoothness in the trailing edge, hence no Brillouin precursor.

Furthermore, in the case of FF-FF, the influence of polarization due to the isotropy (horizontal branch orientation in this case) inherent to the vegetation medium considered in this study is apparent. Moreover, the horizontal branch orientation would impact the HH polarization more than the VV polarization. In Figs. 4 and 5 this result can be noticed in the comparative larger amplitudes shown by the HH cases at the leading and trailing edges depicting Brillouin precursors. This may be due to the fact that the propagating EM wave in HH polarization encounters more wood and branches and less air than that of the VV polarization because of the predominantly horizontal orientation of the branches. Thus, actual medium, in this case a tree, can be seen as a polidispersive medium [14] composed of leafy vegetation, wood, and air, which is non-isotropic. Due to the non-isotropic and polidispersive features, the region illuminated by the antennas becomes critical. In the NF cases, the illuminated region is not only comparatively small it also has more air pockets closer to the trunk of the tree. Thus, the Brillouin precursor formation is weaker for NF positions, as is seen in Fig. 5.

Additionally, the results also seem to be dependent on the receiver antenna FF or NF positions. The propagating signal seems to have more pronounced dispersive effect in NF configuration of the receiver for VV polarization, as shown in Fig. 6.

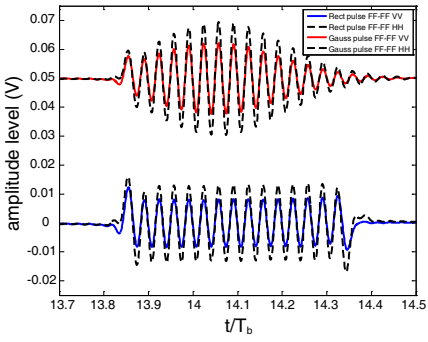

Figure 4. Sine-modulated rectangular (bottom) and Gaussian (top, baseline offset for clarity) pulse after propagating through vegetation, indicating the Brillouin precursor formation for FF-FF configurations.

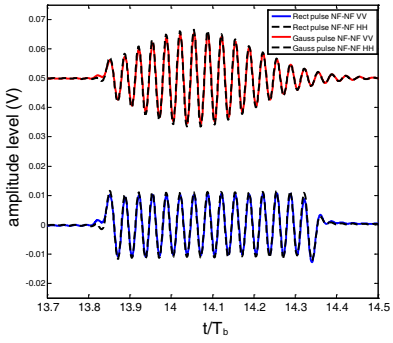

Figure 5. Same parameters as in Fig. 4 for NF-NF configurations.

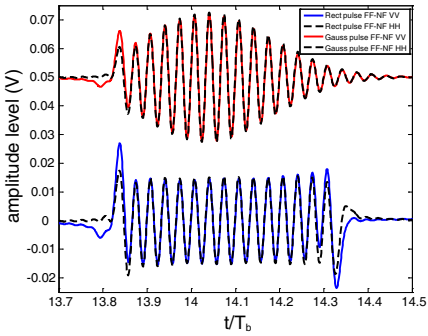

Figure 6. Same parameters as in Fig. 4 for FF-NF configurations.

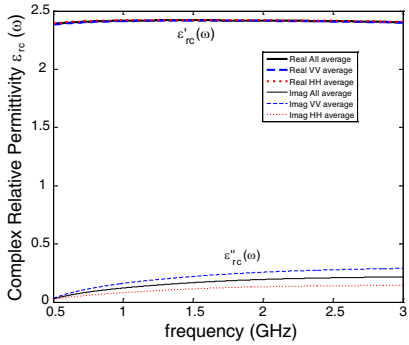

Figure 7. Estimated complex relative permittivity of vegetation used in this study.

4. EVOLUTION OF SEQUENCE OF PULSES

To characterize the evolution of a propagating EM waveform through dispersive media, the above explained method can be used in a generalized form. Additionally, we may estimate the experimental complex dielectric permittivity $\hat{\varepsilon}_r(\omega)$ of the underlying dispersive media using the experimental data. The estimated dielectric permittivity can then be used to predict the behavior of any input signal. In [10], we have introduced a formulation to predict the precursor formation and its evolution within a given dispersive medium [15]. This formulation is based on the fact that a band-limited sine-modulated pulse $x(t)$ can be re-constructed in the time-domain considering only a limited set of $2M+1$ orthogonal frequency components around its carrier frequency, f_0, as in (4):

$$\tilde{x}\,(z,t) = \frac{1}{N}\sum_{k=M_L}^{M_H} |X\,(f_k)| \cdot e^{-\alpha_k z} \cdot \cos\left(2\pi f_k t - \beta_k z + \phi_k\right) \qquad (4)$$

Here $|X(f_k)|$ and $\angle X(f_k) = \phi_k$ are the magnitude and the phase, respectively, corresponding to the kth frequency component at a reference propagation distance $z = 0$; α_k and β_k indicate the attenuation and phase constants for a dispersive medium at the kth frequency component f_k.

The dielectric model assumed to predict the α_k and β_k values will determine the accuracy of the precursor formation and its evolution. A pure Debye model cannot faithfully predict the dielectric permittivity of a complex vegetation media (also considered polidispersive), thereby

necessitating the use of mixed models. Presently used various mixed models for vegetation assume homogeneity and are centered on different forms of the moisture contents within the medium. Actual medium, in this case a tree, assumed a polidispersive medium [14] composed of vegetation and air. Thus, some dielectric models as those given by [16–20] are not valid, and if such models are used, the simulation results can largely be different than that of the actual medium. It is then reasonable to estimate the dielectric parameters of the underlying media experimentally, instead of assuming a generalized model.

The propagation constant, $\gamma_m(\omega)$, and the complex relative permittivity $\hat{\varepsilon}_r(\omega)$, can be estimated using (5):

$$\gamma_m = \alpha_m(\omega) + j\beta_m(\omega) = j\frac{\omega}{c}\sqrt{\hat{\varepsilon}'_{rm}(\omega) - j\hat{\varepsilon}''_{rm}(\omega)} \tag{5}$$

where α_m, and β_m are attenuation and phase constants; $\hat{\varepsilon}'_{r,m}(\omega)$ and $\hat{\varepsilon}''_{r,m}(\omega)$ are real and imaginary parts of the complex relative permittivity of the medium; c is the speed of light in free space, and ω is the frequency in radians. In Fig. 7, we show average $\hat{\varepsilon}'_{r,m}(\omega)$ and $\hat{\varepsilon}''_{r,m}(\omega)$ for all HH and VV configurations as well as the overall averages containing both HH and VV.

Low frequencies, such as 0–0.5 GHz range, can contribute positively to the formation of the Brillouin precursor. This study, however, did not cover that low frequency range due to the antenna bandwidth limitations. In Fig. 8, we the dispersive behavior of vegetation media for a hypothetical broadband communication system at central frequency $f_0 = 2.5$ GHz with a bandwidth of $1/T_b = 250$ MHz, using rectangular and Gaussian pulses. All the amplitudes have been normalized to allow the simultaneous plotting of the pulses, as well as the attenuation and phase constants. The frequency-dependent effect on the attenuation and phase constants are apparent in Fig. 8. It also explains that despite the bandwidth constraint, the dispersive behavior of the vegetation media is large enough to form the precursor, particularly for a rectangular pulse, as shown in Figs. 4–6 and Fig. 9.

Using (4) and the average $\bar{\alpha}_m(\omega)$ and $\bar{\beta}_m(\omega)$ for the HH and VV configurations, the dynamical evolution of a sequence of rectangular pulses through the vegetation medium is plotted in Fig. 9. The formation of precursors may be observed in all configurations, with a considerably larger amplitude level in the FF-NF-VV case. To obtain results in Fig. 9, we have assumed a BPSK modulated pseudo random binary sequence (PRBS) sequence of rectangular pulses with length $M = 15$ bits, carrier frequency $f_0 = 2.5$ GHz, and pulse width $T_b = 10/f_0$.

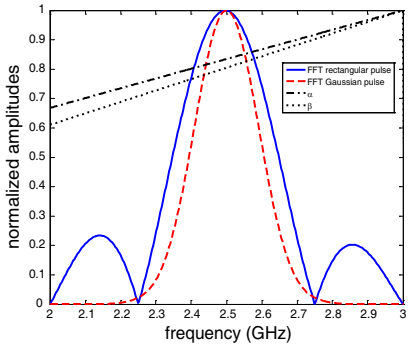

Figure 8. Simultaneous plotting of rectangular and Gaussian pulses, as well as estimated attenuation and phase constants.

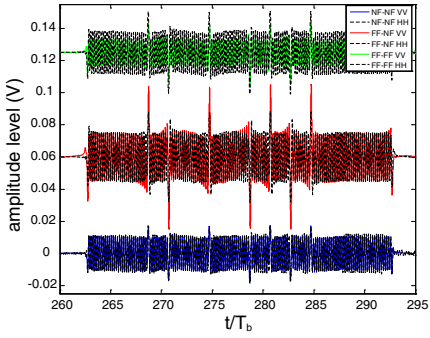

Figure 9. Brilluoin precursor formation for a $M = 15$ PRBS sequence of rectangular pulses for all configurations.

4.1. Spatial Peak Decay Amplitude Estimation

Referring to Fig. 10, the total average propagated field $E_T(t, z)$ follows an algebraically decaying peak amplitude, governed by $0.48 \cdot \Delta z^{-7/9}$ and $0.44 \cdot \Delta z^{-7/8}$, for VV and HH polarizations, respectively. This may be compared with the theoretical simulation in [10] using the Maetzler dielectric model indicating the peak amplitude decay governed by $0.5 \cdot \Delta z^{-2/3}$. It may be reasonable to assume that this difference is mainly due to the effects of the polidispersive nature of the vegetation medium that cannot be modeled as a homogeneous space.

It is also observed in Fig. 10 that the Brillouin precursor formed in the leading and trailing edges of each pulse produces a deformation of the sequence if a bit phase change transition occurs. The phases of the two adjacent bits will determine the peak level cancellation or reinforcement of the two adjacent precursors: cancelled if bit phase continuity takes place and added if bit phase transition occurs [10].

4.2. Polidispersive Fitting of the Total Propagated Field

The total propagated field $E_T(t, z)$ could be thought of as a sum of two components: one undergoing an exponential decay due to the propagation through the air gaps existing between the tree branches; and the other following an algebraic amplitude decay due to the propagation through the vegetation. Therefore, typical theoretical vegetation models, such as the Maetzler model [10, 19], assuming a continuous vegetation may not be suitable for the case

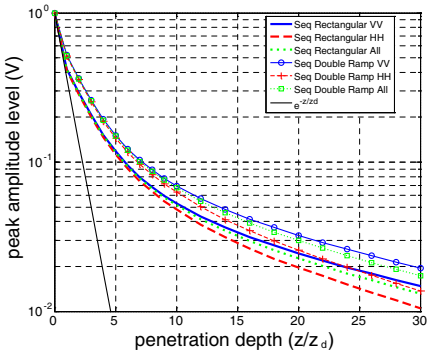

Figure 10. Comparison of peak amplitude decay obtained using theoretical formulation and estimated dielectric permittivity for a $M = 15$ PRBS sequence of rectangular pulses and inverted double ramp pulses for VV, HH and all average configurations.

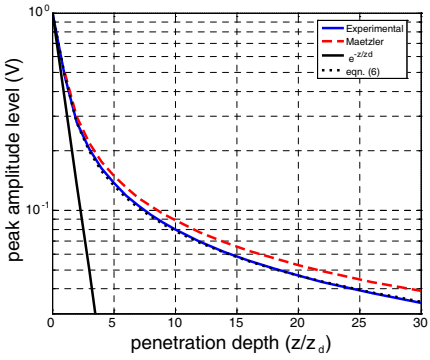

Figure 11. Peak amplitude decay according to polidispersive model for a $M = 15$ PRBS sequence of rectangular pulses.

under investigation. We therefore propose a modified form of the Maetzler [10, 19] model that incorporates the polidispersive features of the media:

$$E_{T\_polidispersive}(t,z) = c \cdot E_{T\_Maetzler}(t,z) + d \cdot e^{-\Delta z} \tag{6}$$

where a and b indicate percentages of each of the above components that must sum to 100% or $c + d = 1$. The model $E_{T\_polidispersive}(t,z)$ in (6) agrees well with experimentally achieved results. For example, using average of all configurations, and $c = 0.885$ and $d = 0.115$ for foliage and air gaps, respectively, the resulting peak amplitude decay is shown in Fig. 11. One can easily note that the discrepancy in using the Maetzler model [10, 19] alone has been corrected by using (6).

4.3. Pulse Width Spreading and Frequency Downshift Estimation

As a pulse propagates through a dispersive media, it undergoes time-width spreading or broadening and frequency downshift [3, 7, 10]. Using the experimentally determined $\hat{\varepsilon}_r(\omega)$ in (5), Fig. 12 illustrates the time-width spreading versus the propagation distance for a PRBS, sine-modulated rectangular pulse sequence of length $M = 15$, $f_0 = 2.5\,\text{GHz}$, and $T_b = 10/f_0 = 1/250\,\text{MHz}$. Fig. 12 also shows the results

that would be theoretically obtained if the Maetzler model is assumed for the dielectric permittivity, as explained in [10]. It may also be noted that the Brillouin precursor undergoes a temporal width change according to $\Delta T_c = T_c \cdot \Delta z/30$, indicating that the sequence would experience a width variation equivalent to one pulse width over a propagation distance of $30 \cdot z_d$. This result is about four times less than the one obtained in [10] using only the theoretical Maetzler model.

5. DYNAMICAL EVOLUTION OF POWER SPECTRUM DENSITY AND BIT ENERGY

Inside the dispersive medium, the total field $E_T(t, z)$ is a sum of two components, namely the Brillouin precursor component, $E_B(t, z)$, and the carrier component, $E_C(t, z)$. The carrier component $E_C(t, z)$ is governed by the typical exponential decay, whereas the Brillouin precursor component $E_B(t, z)$ decays algebraically. In Fig. 13, we have plotted the average power of one $M = 15$ PRBS sequence of sine-modulated rectangular pulses at $f_0 = 2.5\,\text{GHz}$ with $T_b = 10/f_0 = 1/250\,\text{MHz}$. This average power has been calculated using the integral of the PSD over the bandwidth $[f_0 - 1/T_b, f_0 + 1/T_b]$. After a penetration depth of $z = 2 \cdot z_d$, we observe that the average power also experiences an algebraic decay, clearly showing the advantageous behavior of the Brillouin precursor in terms of power.

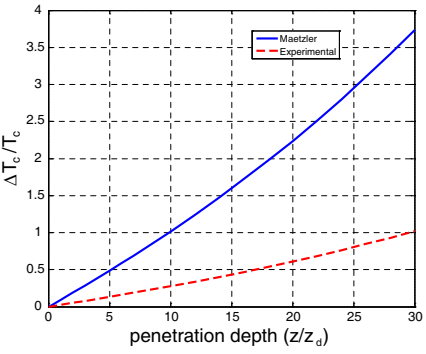

Figure 12. Width spreading experienced by a $M = 15$ PRBS sequence of rectangular pulses.

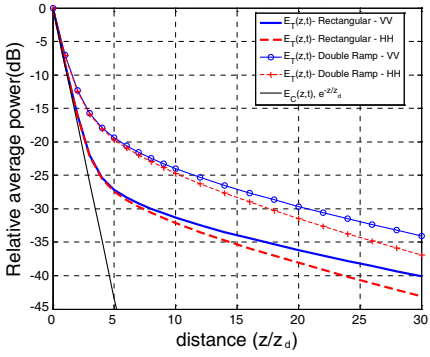

Figure 13. Comparison of relative average power evolution for a $M = 15$ PRBS sequence of rectangular pulses and inverted double ramp pulses for VV and HH configurations.

Similarly, Fig. 14 describes the bit energy E_b for the same parameters used for Fig. 13. It represents the average E_b for the sequence, since only some bits contain precursors. It also shows the same trend as that of the average power in Fig. 13. The E_b was estimated using a demodulated BPSK signal as shown in [10]. The plotted E_b corresponds to the average of the single E_b of each bit of the sequence. The same is also compared using the exponentially decaying model $e^{-2\alpha(f_0)}$. It may be inferred that the larger the penetration depth, the greater is the bit energy compared to that of the carrier component, containing almost all of the energy in the Brillouin component after $z = 2 \cdot z_d$.

The results in Fig. 14 and the associated phenomenon of algebraic decay are useful to improve the signal-to-noise (SNR) or E_b/N_0 ratio, thereby improving the BER. For example, for $z = 5 \cdot z_d$, we have a bit energy of 1.44×10^{-3} mW (E_{b_B}) compared to 4.5×10^{-5} mW (E_{b_I}) of the exponentially decaying case. Assuming an additive white Gaussian noise, the bit error rate (BER) could be 6.4×10^{-29} for E_{b_B} and 2.5×10^{-22} for E_{b_I}, given a noise PSD of $N_0 = K \cdot T \cdot B = 10^{-12}$, $K = 1.38065 \times 10^{-23}$ [J/K] the Boltzman constant, $T = 290$ F, and $B = 250$ MHz, the receiver bandwidth.

6. NEAR-OPTIMAL WAVEFORM FOR BIT SEQUENCES

For PRBS sequences, we propose a near-optimal waveform for traveling through a dispersive medium such as vegetation. It consists of an inverse double ramp pulse. Unlike the sequences of rectangular pulses, the Brillouin precursor takes place in the middle of each pulse, so no cancelation occurs when there is a phase transition in adjacent bits. The suggested input pulse f_{DS} consists of a structure of one positive and one negative cycle without any transition between cycles as in (7):

$$f_{DS}(t) = \begin{cases} \dfrac{1}{t_r} \cdot t & 0 \le t \le t_r \\ \dfrac{1}{t_f - t_r} \cdot (t - t_r) & t_r \le t \le t_f \end{cases} \tag{7}$$

with t_r and t_f the rising and falling times, in our case $t_r = t_f = T_b/2$.

In Fig. 15, we depict the propagation of a $M = 15$ PRBS sequence of inverted double ramp sine-modulated pulses according to (7), with $f_0 = 2.5$ GHz, and pulse width $T_b = 10/f_0$, for a propagation distance of $z = 3 \cdot z_d$. These results were obtained using the theoretical simulation and the experimental dielectric permittivity, as explained in Section 4.

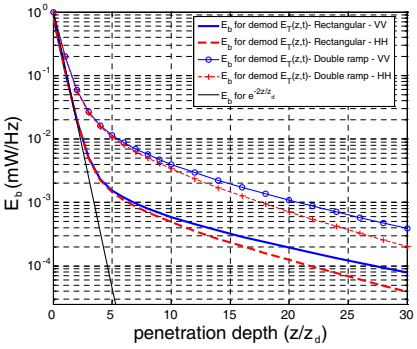

Figure 14. Comparison of bit energy Eb evolution for a $M = 15$ PRBS sequence of rectangular pulses and inverted double ramp pulses for VV and HH configurations.

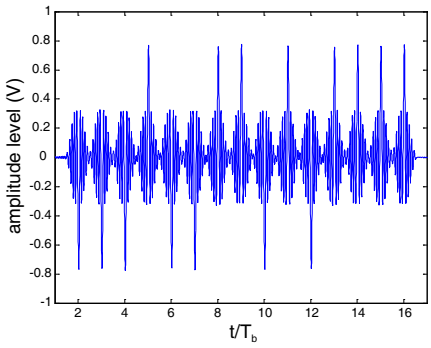

Figure 15. Brilluoin precursor formation for a $M = 15$ PRBS sequence of inverted double ramp pulses for average of all configurations after a propagation distance of $z = 3 \cdot z_d$ within the vegetation sample.

Usually, waveforms based on such a double cycle structure offer larger precursor peak amplitudes due to a rich spread of frequency components, thereby offering an improved peak amplitude decay rate of $0.55 \cdot \Delta z^{-6/7}$ (all, VV) and $0.54 \cdot \Delta z^{-7/8}$ (HH), for the total field $E_T(t, z)$, as can be seen in Fig. 10. This fact is also reflected in the dynamical evolution of the both average power and bit energy, as shown in Fig. 13 and Fig. 14.

In Fig. 10, the double ramp sequence undergoes comparatively less attenuation due to the formation of the Brillouin precursor in each bit. For the same reason, in Fig. 13, this sequence contains comparatively more average power. And according to the results in Fig. 14, we may state that it retains more energy per bit.

Since time spreading occurs only in the middle of the pulse where the leading edge is located, it does not impact the overall pulse and so the sequence does not experience any broadening. This is an additional advantage over the rectangular case.

7. CONCLUSIONS

An experimental method using frequency-dependent propagation characteristics of the dispersive material has been extended to observe the Brillouin precursor in leafy vegetation. The result is a frequency filter $Ts_{21}(f)$ that incorporates the attenuation and the phase

distortion effects on EM waves propagating through the dispersive vegetation. Sine-modulated input signals consisting of rectangular and Gaussian pulses were used in this experimental method. The results presented herein are of great importance to predict the maximum penetration distance for any kind of input waveforms used within the dielectric medium considered in this study. It may also be noted that the vegetation should be modeled with non-homogeneous and polidispersive features.

The experimental data were also used to estimate the complex relative permittivity of the vegetation sample. This estimated permittivity can then be used in the theoretical formulation based on the Discrete Fourier Transform decomposition, to analyze the dynamical evolution of any kind of input waveform. This formulation facilitated the achievement of theoretical analysis and its comparison with experimental results. Nevertheless, ongoing research should be kept in the line of asymptotic method to provide closed-form solution to some points related to the Brillouin precursor analysis, as shown in [4]. Other methods, such as the Finite Difference Time Domain (FDTD) [21] have also demonstrated potential to model the dispersive phenomenon. This latter method has yet to solve many challenges as indicated in [15].

We have shown the reconstructed Brillouin precursors for a sequence of rectangular pulses using the method outlined in this paper. The classical rectangular pulse sequence has been shown to obey non-exponentially peak amplitude attenuation versus the distance traveled through the dispersive medium. The power spectrum density and the bit energy evolution are introduced as one of the many aspects regarding the evolution of the precursor waveforms through the leafy vegetation, showing the advantageous effects of precursor formation through the vegetation [10, 22]. Many applications, such as path-loss propagation models in forested environments [23] or ground penetrating radar [24], could take advantage of the precursor presence to improve their performance.

Furthermore, the frequency dependent behavior of $\bar{\alpha}_m(\omega)$ and $\bar{\beta}_m(\omega)$, together with the correct selection of indexes M_L and M_H in (4), in order to include the largest possible amount of signal energy over the bandwidth of interest, are sufficient conditions to guarantee the observation of Brillouin precursor formation despite of the bandwidth constraint.

Finally, a near-optimal pulse is proposed as a solution to contain the time broadening aspect of a pulse traveling through a dispersive medium. This near-optimal pulse ensures the presence of the Brillouin precursor in each bit of the sequence, thereby retaining more average

power and bit energy and, hence, larger propagation distance, and/or better BER.

ACKNOWLEDGMENT

This work was partly supported by the New Mexico State University (NMSU), Las Cruces, NM, USA, and a NMSU patent is pending. We would also like to acknowledge the support of National Science Foundation (NSF) through the Bridge to Doctorate program, and the support received from the People Program of 7th FrameWork Programme (2008 Marie Curie IOF Action).

REFERENCES

1. Uduwawala, D., M. Norgren, P. Fuks, and A. Gunawardena, "A complete FDTD simulation of a real GPR antenna system operating above lossy and dispersive grounds," *Progress In Electromagnetics Research*, Vol. 50, 209–229, 2005.
2. Hillion, P., "Electromagnetic pulse propagation in dispersive media," *Progress In Electromagnetics Research*, Vol. 35, 299–314, 2002.
3. Oughstun, K. E. and G. C. Sherman, *Electromagnetic and Optical Pulse Propagation*, Vol. 2, Springer-Verlag, Berlin, Germany, 2009.
4. Oughstun, K. E., "Dynamical evolution of the Brillouin precursor in Rocard-Powles-Debye model dielectrics," *IEEE Transactions on Antennas and Propagation*, Vol. 53, No. 5, 1582–1590, 2005.
5. Pleshko, P. and I. Palózc, "Experimental observation of Sommerfeld and Brillouin precursors in the microwave domain," *Physical Review Letters*, Vol. 22, No. 22, June 1969.
6. Liu, S.-H., C.-H. Liang, W. Ding, L. Chen, and W.-T. Pan, "Electromagnetic wave propagation through a slab waveguide of uniaxially anisotropic dispersive metamaterial," *Progress In Electromagnetics Research*, Vol. 76, 467–475, 2007.
7. Mohammed, H., M. Dawood, and A. Alejos, "Experimental detection of brillouin precursors through tap water at microwave frequencies," in review for *IET Electronics Letters*, July 2010.
8. Chen, L. F., C. K. Ong, C. P. Neo, V. V. Varadan, and V. K. Varadan, *Microwave Electronics: Measurement and Materials Characterization*, Wiley, 2004.
9. Hasar, U. C., "Unique permittivity determination of low-loss dielectric materials from transmission measurements at microwave

frequencies," *Progress In Electromagnetics Research*, Vol. 107, 31–46, 2010.

10. Alejos, A. V., M. Dawood, and H. U. R. Mohammed, "Analysis of Brillouin precursor propagation through foliage for digital sequences of pulses," *IEEE Geosci. Remote Sensing Letters*, Vol. 8, No. 1, 59–63, January 2011.
11. Heidari, A., M. Neshat, D. Saeedkia, and S. Safavi-Naeini, "Signal recovery in pulsed terahertz integrated circuits," *Progress In Electromagnetics Research*, Vol. 107, 269–292, 2010.
12. Alejos, A. V., M. G. Sanchez, and I. Cuiñas, "Measurement and analysis of propagation mechanisms at 40 GHz: Viability of site shielding forced by obstacles," *IEEE Transactions on Vehicular Technology*, Vol. 58, No. 2, 3369–3380, 2008.
13. Correia, L. M. and P. O. Françês, "Transmission and isolation of signals in buildings at 60 GHz," *Int. Symp. on Personal, Indoor and Mobile Communications, (PIMRC)*, Toronto, Canada, September 1995.
14. Chukhlantsev, A., A. Shutko, S. Golovachev, and A. Chukhlantsev, "Conductivity of leaves and branches and its relation to the spectral dependence of attenuation by forests in meter and decimeter band," *Intern. Geosci. Remote Sensing Symposium*, Vol. 2, 1103–1105, 2003.
15. Luebbers, R., T. Uno, and K. Kumagai, "Comments on 'Pulse propagation in a linear, causally dispersive medium'," *Proceedings of the IEEE*, Vol. 81, No. 4, 1993.
16. Fung, A. K. and F. T. Ulaby, "A scatter model for leafy vegetation," *IEEE Trans. Geosci. Electron.*, Vol. 16, 281–286, 1978.
17. El Rayes, M. A. and F. T. Ulaby, "Microwave dielectric spectrum of vegetation, part II: Dual dispersion model," *IEEE Trans. Geoscience Remote Sensing*, Vol. 25, 550–557, Sep. 1987.
18. Brown, G. S. and W. J. Curry, "A theory and model for wave propagation through foliage," *Radio Science*, Vol. 17, No. 5, 1027–1036, 1982.
19. Maetzler, C., "Microwave (1–100 GHz) dielectric model of leaves," *IEEE Trans. Geosci. Remote Sensing*, Vol. 33, 947–949, 1994.
20. Pearce, C., "The permittivity of two phase mixtures," *Brit. J. Applied Physics*, Vol. 61, 358–361, 1955.
21. Wei, B., S.-Q. Zhang, Y.-H. Dong, and F. Wang, "A general FDTD algorithm handling thin dispersive layer," *Progress In Electromagnetics Research B*, Vol. 18, 243–257, 2009.

22. Oughstun, K. E., "On the use & application of precursor waveforms," *13th International Symposium on Antenna Technology and Applied Electromagnetics and the Canadian Radio Sciences Meeting, (ANTEM/URSI)*, Banff, Alberta, Canada, February 15–18, 2009.
23. Li, Y. and H. Ling, "Numerical modeling and mechanism analysis of VHF wave propagation in forested environments using the equivalent slab model," *Progress In Electromagnetics Research*, Vol. 91, 17–34, 2009.
24. Capineri, L., D. J. Daniels, P. Falorni, O. L. Lopera, and C. G. Windsor, "Estimation of relative permittivity of shallow soils by using the ground penetrating radar response from different buried targets," *Progress In Electromagnetics Research Letters*, Vol. 2, 63–71, 2008.